Celestial Mechanics and Dynamical Astronomy manuscript No.
(will be inserted by the editor)

G. Mingotti · F. Topputo · F. Bernelli-Zazzera

Earth–Mars Transfers with Ballistic Escape and Low-Thrust Capture*

Received: date / Accepted: date

Abstract In this paper novel Earth–Mars transfers are presented. These transfers exploit the natural dynamics of n-body models as well as the high specific impulse typical of low-thrust systems. The Moon-perturbed version of the Sun–Earth problem is introduced to design ballistic escape orbits performing lunar gravity assists. The ballistic capture is designed in the Sun–Mars system where special attainable sets are defined and used to handle the low-thrust control. The complete trajectory is optimized in the full n-body problem which takes into account planets' orbital inclinations and eccentricities. Accurate, efficient solutions with reasonable flight times are presented and compared with known results.

1 Introduction

Low energy transfers outperform classic patched-conics orbits in terms of propellant mass [1]. The natural dynamics embedded in the n-body problems is exploited in these transfers. In particular, the ballistic capture mechanism avoids having hyperbolic excess velocities, so reducing the cost needed to insert the spacecraft into a final, stable orbit about the arrival planet [2]. Low energy transfers can also be thought under the perspective of Lagrangian point orbits and their invariant manifolds [3–11]. In this case, the structure of the phase space about the collinear points of the restricted three-body problem is used to define efficient coast arcs. Trajectories obtained adopting two distinct three-body systems are matched together to define the transfer orbit. This technique is labeled "patched restricted three-body problems approximation" and represents a sophisticated update to the patched-conics method. Ballistic escape can be used besides ballistic capture to

* Part of the work described in this paper has been presented at the 61st International Astronautical Congress, Prague, Czech Republic, 27 September – 1 October 2010.

Giorgio Mingotti
Universität Paderborn, Institute für Industriemathematik
Warburger Str. 100, – 33098, Paderborn, Germany
Tel.: +49-5251-60-5015; Fax: +49-5251-60-5020
E-mail: giorgio.mingotti@mail.polimi.it

Francesco Topputo, Franco Bernelli-Zazzera
Politecnico di Milano, Dipartimento di Ingegneria Aerospaziale
Via La Masa, 34 – 20156, Milano, Italy
Tel.: +39-02-2399-8640/8328; Fax: +39-02-2399-8334
E-mail: {francesco.topputo, franco.bernelli}@polimi.it

further enhance the trajectory performances. This is a mechanism equivalent to ballistic capture, and it is usually defined in a four-body model [12, 13].

The chemical, patched restricted three-body problems approximation requires that the manifolds of the two systems intersect in the configuration space. This occurs in the Sun–Earth–Moon scenario (in constructing Earth–Moon transfers) as well as in transfers between outer planets and their moons [4,6,7,14]. No intersection exists among manifolds of inner planets. A method to design Earth–Mars transfers exploiting the Lagrangian point dynamics has been formulated in [11]; this is called "patched conic-manifolds" method. All these methods are based on instantaneous velocity changes needed to connect the manifolds of two systems in the phase space. Low-thrust propulsion is proposed in this paper to further improve the performances of low energy transfers. As existing methods rely on impulsive maneuvers, the design strategy needs to be modified to accommodate low-thrust control. This is done by defining special attainable sets. In short, an attainable set is a collection of low-thrust orbits that are propagated from a set of admissible initial conditions, with a specified guidance law and for a specified time. As the patched three-body problems approximation requires the intersection of the manifolds, and this condition is not verified in the Earth–Mars context [11, 15], the idea behind our approach is to replace invariant manifolds with attainable sets, and to manipulate the latter in the same way the manifolds are used to define space trajectories. Low-energy, low-thrust Earth–Mars transfers are so formulated. Not only the intrinsic dynamics of n-body problems is exploited, but also the high specific impulse of low-thrust systems is utilized in order to define efficient trajectories. These transfers are made up by a ballistic escape portion and a low-thrust capture. Ballistic escape is defined in the Moon-perturbed Sun–Earth model; low-thrust capture is instead defined in the Sun–Mars problem. These two pieces are joined and optimized in the controlled n-body problem. In this model, the spacecraft's low-thrust propulsion as well as the planet's gravitational attractions are taken into account. The low-thrust represents the control term as it is used to adjust the natural flow of the n-body equations of motion. This paper follows previous works by the same authors aimed at combining dynamical system theory and optimal control problems to design efficient space trajectories [16, 17].

The literature on low-thrust, n-body trajectories is vast. A spiral arc is matched to a Moon transit orbit in [18] (this concept has been later implemented in ESA's SMART-1 mission [19]). The use of invariant manifolds as first guess to initiate low-thrust optimization is described in [20]. Capture and escape orbits have been obtained with sophisticated optimization algorithms in [21]. Low-thrust propulsion has been used within the restricted three-body problem to design both interplanetary transfers [22–24] and transfers to the Moon [25, 26]. Low-thrust, stable-manifold transfers to halo orbits are also shown in [27–33]. Lunar gravity assists at departure in the frame of Earth–Mars transfers have been proposed in [34].

1.1 Summary of the Approach

The approach is briefly sketched for the sake of clarity (details are given throughout the paper). To construct a chemical, low-energy transfer between the Earth and Mars, it is required that the invariant manifolds of the two restricted three-body problems (Sun–Earth and Sun–Mars models) intersect at least in the position space. Given the problem geometry, the unstable manifold of the L_2 orbits is considered in the Sun–Earth problem ($W^u_{L_2}$ SE), and the stable manifold of the L_1 orbits is considered in the Sun–Mars problem ($W^s_{L_1}$ SM). If these intersected, an Earth–Mars low energy transfer with at most one deep-space maneuver would exist. Unfortunately, these two objects do not intersect, and this can be viewed on a common surface of section in Fig. 1(a) where the two manifolds are reported in the Sun–Earth rotating frame. A first attempt to get the two sets closer consists in the introduction of a lunar gravity assist at departure. The associated ballistic escape orbits, defined in the Moon-perturbed Sun–Earth problem, are represented by the dashed line in Fig. 1(b). Although the lunar gravity assist moves the set of ballistic escape orbits

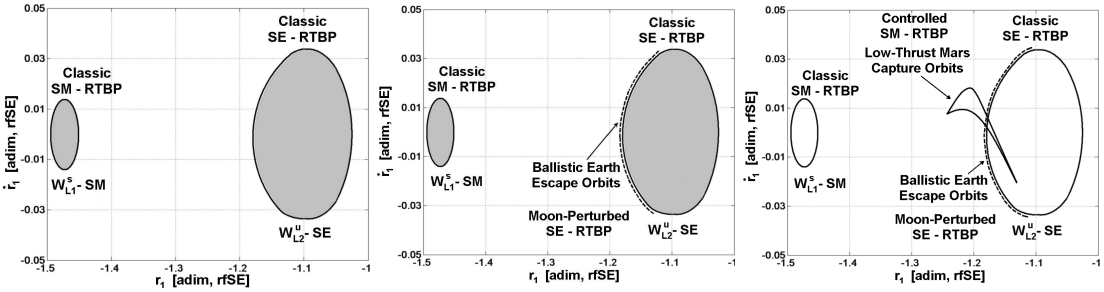

(a) Non-intersecting manifolds. (b) Effect of lunar gravity assist. (c) Effect of low-thrust capture.

Fig. 1 Summary of the approach. Given the two non-intersecting manifolds (Fig. 1(a)) defined into two restricted three-body problems, the Moon-perturbed Sun–Earth problem is introduced to design ballistic escape orbits exploiting lunar gravity assist (Fig. 1(b), dashed line). This set is then connected with the low-thrust capture orbits obtained in the controlled Sun–Mars problem (Fig. 1(c)). The intersection between ballistic escape and low-thrust capture sets uniquely specifies a first guess solution which is later optimized in the controlled, restricted n-body problem.

towards the Sun–Mars manifold, it is not enough to perform the intersection. Such intersection can be achieved when low-thrust propulsion is introduced. The low-thrust capture set in Fig. 1(c) is obtained in the controlled Sun–Mars problem with tangential thrust as detailed in Section 3.2. The intersection between this set and the ballistic escape orbits defines the transfer point. (Note that the low-thrust capture set intersects also the L_2 orbits unstable manifold; nevertheless, considering its intersection with orbits flying-by the Moon produces solutions requiring less propellant). This point uniquely identifies a first guess transfer orbit which is later optimized in the controlled, restricted n-body problem.

The paper is organized as follows. In Section 2 the problem is stated and some background notions to design ballistic capture and escape orbits using the Lagrangian points dynamics are recalled. In the same section the Moon-perturbed Sun–Earth model is presented. Section 3 introduces the low-thrust propulsion into the restricted three-body problem and defines the attainable sets. In Section 4 the design strategy is formulated: ballistic escape orbits and Mars low-thrust capture trajectories are matched together. The complete transfer optimization is defined in Section 5 and the obtained results are discussed in Section 6. Concluding remarks are given in Section 7.

2 Background

2.1 Statement of the Problem

In the linked-conics method used in interplanetary trajectory design, the spacecraft motion is studied outside of the spheres of influence of the planets, and heliocentric rendez-vous transfers are treated. In the patched-conics approximation, the two-body motion about the planets is studied, and the associated solutions are connected using the concept of sphere of influence [35]. Interplanetary trajectories considered in this work connect an orbit around the Earth with an orbit around Mars. Planet-centered frameworks are indeed considered to exploit the three- and four-body dynamics governing ballistic capture and escape. This can be thought as a refinement of both linked- and patched-conics methods.

The spacecraft is assumed to be initially on a circular parking orbit around the Earth at a given altitude h_E. An initial impulsive maneuver, whose magnitude is Δv_E, is provided to

place the spacecraft on a trajectory that escapes from the Earth. The energy level of this Earth-escaping orbit is lower than that associated to two-body trans-Mars injection hyperbolas. In addition, this trajectory exploits the gravitational attractions of the Sun, Earth, and Moon. For these reasons this phase is called *ballistic escape*.

After the launch, the spacecraft can only rely on its own low-thrust propulsion to rendezvous with Mars and to descend down to a stable orbit around it. This phase is called *low-thrust capture* as the Sun–Mars interaction is exploited (besides the low-thrust) to reach the final orbit. The final orbit has eccentricity, e, and periapsis (or apoapsis), r_p (or r_a), prescribed by mission requirements. The transfer is assumed to terminate when the spacecraft reaches the periapsis of the final orbit. Three out of the four parameters needed to specify an orbit in a planar context are given. The fourth (orbit orientation, ω) is determined in the trajectory optimization.

As both chemical and low-thrust propulsions are considered, our approach may also be labelled as producing *hybrid propulsion* transfers.

2.2 The Planar Circular Restricted Three-Body Problem

The motion of the spacecraft, P_3, of mass m_3, is studied in the gravitational field generated by two primaries, P_1, P_2, of masses m_1, m_2, respectively, assumed to move in circular motion about their common center of mass (Fig. 2(a)). It is assumed that P_3 moves in the same plane of P_1, P_2 under the equations [36]

$$\ddot{x} - 2\dot{y} = \frac{\partial \Omega}{\partial x}, \qquad \ddot{y} + 2\dot{x} = \frac{\partial \Omega}{\partial y}, \tag{1}$$

where the auxiliary function is

$$\Omega(x, y, \mu) = \frac{1}{2}(x^2 + y^2) + \frac{1-\mu}{r_1} + \frac{\mu}{r_2} + \frac{1}{2}\mu(1-\mu), \tag{2}$$

and $\mu = m_2/(m_1 + m_2)$ is the mass parameter of the three-body problem. Eqs. (1) are written in a barycentric rotating frame with nondimensional units: the angular velocity of P_1, P_2, their distance, and the sum of their masses are all set to the unit value. Thus, P_1, P_2 have scaled masses $1-\mu$, μ, and are located at $(-\mu, 0)$, $(1-\mu, 0)$, respectively. The distances in Eq. (2) are therefore

$$r_1^2 = (x+\mu)^2 + y^2, \qquad r_2^2 = (x+\mu-1)^2 + y^2. \tag{3}$$

For fixed μ, the energy of P_3 is represented by the Jacobi integral which reads

$$J(x, y, \dot{x}, \dot{y}) = 2\Omega(x, y) - (\dot{x}^2 + \dot{y}^2), \tag{4}$$

and, for a given energy C, it defines a three-dimensional manifold

$$\mathcal{J}(C) = \{(x, y, \dot{x}, \dot{y}) \in \mathbb{R}^4 \,|\, J(x, y, \dot{x}, \dot{y}) - C = 0\}. \tag{5}$$

The projection of $\mathcal{J}$ on the configuration space (x, y) defines the Hill's curves bounding the allowed and forbidden regions of motion associated with prescribed values of C. The restricted three-body problem (RTBP) has five well-known equilibrium points, L_j, whose energy is C_j, $j = 1, \ldots, 5$. This study considers the dynamics of the two collinear points L_1 and L_2, that behave, linearly, as a saddle $\times$ center. There exists a family of retrograde Lyapunov orbits around L_1, L_2, and two-dimensional stable and unstable manifolds emanating from them [36–38].

The RTBP is used alternatively to model the spacecraft motion in the Sun–Earth (SE) and Sun–Mars (SM) systems, whose mass parameters are $\mu_{SE} = 3.0034 \times 10^{-6}$ and $\mu_{SM} = 3.2268 \times 10^{-7}$, respectively. As for the SE model, the generic periodic orbit about Lj, $j = 1, 2$, is referred to as γ_j, whereas its stable and unstable manifolds are labeled $W^s(\gamma_j)$, $W^u(\gamma_j)$, respectively. In the SM model, the periodic orbits are called λ_j and their manifolds are $W^s(\lambda_j)$, $W^u(\lambda_j)$, $j = 1, 2$.

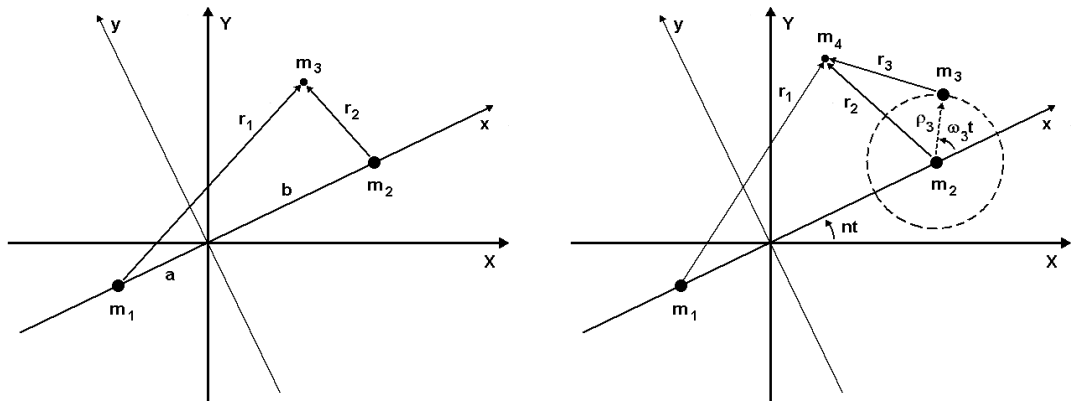

(a) Planar circular RTBP. (b) Moon-perturbed Sun–Earth problem.

Fig. 2 Three- and four-body problems described in Sections 2.2 and 2.3.

2.3 The Moon-perturbed Sun–Earth Model

When the RTBP is used to model the motion in the Sun–Earth system, the Moon is considered with the Earth as a whole. In this case, P_2 is the Earth–Moon barycenter and m_2 considers the masses of the Earth and the Moon. Merging the Earth and the Moon is a good approximation, and in general works well. However, it would be desirable to explicitly exploit the presence of the Moon, at least in its neighborhood. Ballistic escape trajectories may take advantage of Moon gravity assists to reduce the trans-Mars injection cost [34]. Therefore, a Moon-perturbed Sun–Earth problem is formulated. This model preserves the structure of the SE RTBP, and considers the lunar perturbation in the same way the Sun-perturbed Earth–Moon model is formulated in literature [39]. Some assumptions are made: (i) the Sun, the Earth, and the Moon orbit in the same plane; (ii) the Sun and the Earth move on circular orbits around their center of mass; (iii) the Moon moves in a circular orbit around the Earth (Fig. 2(b)). With these assumptions the model is not coherent but it catches basic dynamics of the restricted four-body problem (RFBP) as the primaries have low eccentricities (0.0167 and 0.0549 for the Earth and Moon, respectively) and the Moon is inclined on the ecliptic by 5 deg.

The equations of motion of this RFBP are

$$\ddot{x} - 2\dot{y} = \frac{\partial \Omega_M}{\partial x}, \qquad \ddot{y} + 2\dot{x} = \frac{\partial \Omega_M}{\partial y}, \qquad \dot{\theta} = \omega_M \tag{6}$$

with

$$\Omega_M(x, y, \theta) = \Omega(x, y, \mu_{SE}) + \frac{m_M}{r_M} - \frac{m_M}{\rho_M^2}\,(x\cos\theta + y\sin\theta). \tag{7}$$

The last term in Eq. (7) considers the fact that the Moon does not orbit around a fixed Earth, but both the Earth and the Moon rotate around their common center of mass. The dimensionless physical constants introduced to describe the Moon influence are in agreement with those of the SE model. These are derived starting from primitive values [40]. Thus, the scaled distance between the Moon and the Earth is $\rho_M = \rho_3/l = 2.5721 \times 10^{-3}$, where ρ_3 is the Earth–Moon distance and l is the Sun–Earth distance; the scaled mass of the Moon is $m_M = m_3/(m_1+m_2) = 3.6942 \times 10^{-8}$, where m_1, m_2, and m_3 are the masses of the Sun, the Earth, and the Moon, respectively; the angular velocity of the Moon is $\omega_M = \overline{\omega}_M/n - 1 = 1.2367 \times 10^{1}$, where $\overline{\omega}_M$ and n are the angular velocities of the Earth–Moon and Sun–Earth systems, respectively [17]. The instantaneous location of the Moon is $(1 - \mu_{SE} + \rho_M \cos\theta, \rho_M \sin\theta)$, such that the distance

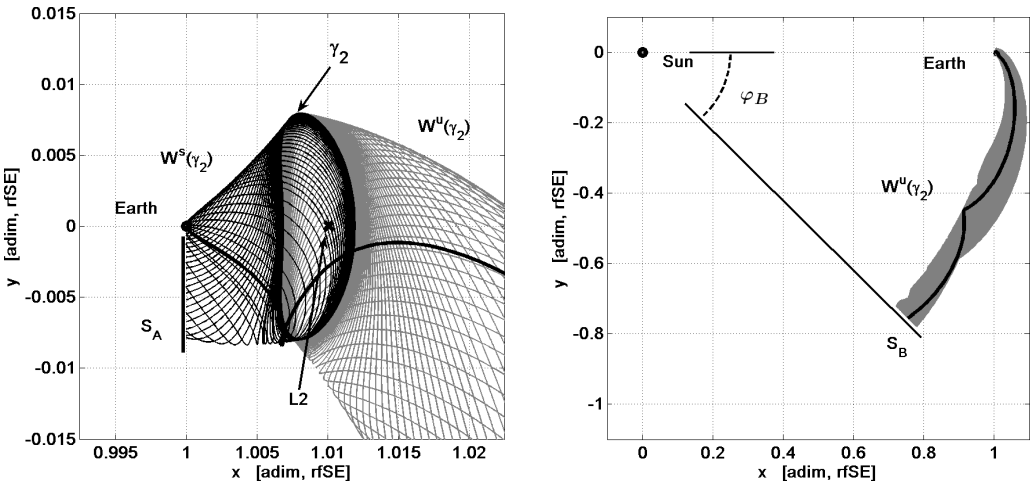

(a) $W^s(\gamma_2)$ and $W^u(\gamma_2)$. (b) $W^u(\gamma_2)$.

Fig. 3 Stable and unstable manifolds $W^s(\gamma_2)$, $W^u(\gamma_2)$, and a sample ballistic escape orbit.

between P_3 and the Moon is

$$r_M^2 = (x - 1 + \mu_{SE} - \rho_M \cos\theta)^2 + (y - \rho_M \sin\theta)^2. \tag{8}$$

Equilibrium points, periodic orbits around them, their invariant manifolds, and the Jacobi integral disappear when Eqs. (6) are considered. This also causes the loss of geometrical properties of the phase space in the libration points region: the separatrix role of the invariant manifolds [5,6] no longer applies. The reader can refer to [17] for the derivation of equations (6)–(8).

2.4 Ballistic Escape from the Earth

In the SE model, an energy value $C_{SE} \lesssim C_2$ is fixed such that γ_1, γ_2 exist, and the Hill's regions are opened at both L_1 and L_2. The periodic orbits and their invariant manifolds, $W^{s,u}(\gamma_{1,2})$, can be computed with standard algorithms [41, 42]. In the following, we construct a ballistic escape orbit exploiting $W^s(\gamma_2)$ and $W^u(\gamma_2)$ in the same way translunar orbits are obtained in Earth–Moon low energy transfers. The reader can refer to [25] for details.

Two surfaces of section are introduced to study the cuts of $W^s(\gamma_2)$, $W^u(\gamma_2)$ (Fig. 3). Section S_A, making an angle φ_A (clockwise) with the x-axis and passing through the Earth, is considered to cut $W^s(\gamma_2)$ (in Fig. 3(a), $\varphi_A = \pi/2$). Section S_B, inclined by φ_B (clockwise) from the x-axis and passing through the Sun, is assumed for $W^u(\gamma_2)$ (in Fig. 3(b), $\varphi_B = \pi/4$). Cutting $W^s(\gamma_2)$, $W^u(\gamma_2)$ with S_A, S_B produces the curves $\partial\Gamma_2^s$, $\partial\Gamma_2^u$ which are diffeomorphic to circles [5, 6]. (For some values of C_{SE} and φ_A, $W^s(\gamma_2)$ may experience close encounters or collisions with the Earth; in this case its section curve is no longer a circle). These cuts can be represented in $(r_2, \dot{r}_2)$ and $(r_1, \dot{r}_1)$ coordinates, respectively (in Fig. 4(b), $\partial\Gamma_2^s$ is reported). Both sections represent two-dimensional maps for the flow of the RTBP. Indeed, any point on these sections uniquely defines an orbit. This property holds as $\mathcal{J}(C_{SE})$ and $S_{A,B}$ lower the dimension of the phase space by two. By definition, points on $\partial\Gamma_2^s$ originate orbits that asymptotically approach γ_2 in forward time. Points inside $\partial\Gamma_2^s$ generate transit orbits that pass from the Earth region to the exterior region, whereas points outside Γ_2^s correspond to nontransit orbits (the manifolds act as separatrices for the states of motion [5, 37, 38]).

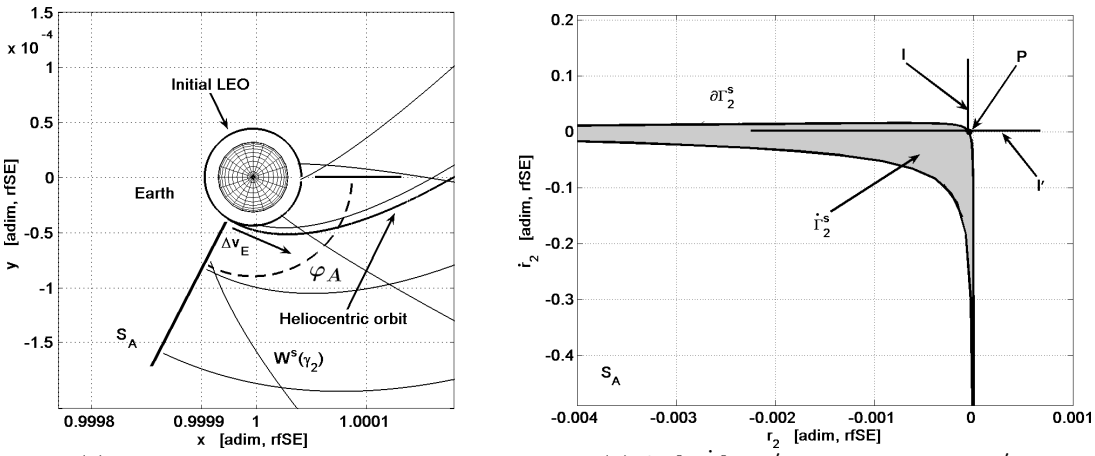

(a) Initial maneuver geometry.

(b) $\partial\Gamma_2^s$, $\dot{\Gamma}_2^s$, l, l', and point $P = l \cap l'$.

Fig. 4 Ballistic escape trajectory performed with a tangential Δv_E maneuver and its associated section point P.

Ballistic escape takes place on orbits inside both $W^s(\gamma_2)$ and $W^u(\gamma_2)$. Let $\dot{\Gamma}_2^s$ be the set of points in the $(r_2, \dot{r}_2)$-plane that are enclosed by $\partial\Gamma_2^s$ (see Fig. 4(b)). Points on $\dot{\Gamma}_2^s$ are of interest. More specifically, all points lying on

$$l = \{(r_2, \dot{r}_2) \in S_A,\, (r_2, \dot{r}_2) \in \dot{\Gamma}_2^s | r_2 = R_E + h_E\} \tag{9}$$

are ballistic escape orbits that intersect the initial parking orbit (R_E is the radius of the Earth). This intersection happens only in the position space, as the initial parking orbit and the escape trajectory show two different energy levels.

The pair $\{C_{SE},\, \varphi_A\}$ uniquely defines the curve $\partial\Gamma_2^s$ on S_A (C_{SE} defines the orbit γ_2; φ_A defines the surface S_A to cut $W^s(\gamma_2)$). It can be shown that $\{C_{SE},\, \varphi_A\}$ may be suitably tuned to produce transit orbits tangent to the Earth-parking orbit [25]. Typical values of Jacobi constant range in the interval $C_{SE} \in [3.0001,\, 3.0002]$ ($C_2 \simeq 3.0008$ in the SE model); as for the surface of section, $\varphi_A \in [\pi/2,\, 3/2\pi]$. With reference to Figure 4(a), these values guarantee that the stable manifold $W^s(\gamma_2)$, backward integrated, is tangent to the parking orbit; this yields tangential insertion maneuvers: the initial Δv_E is aligned with the velocity of the circular parking orbit. The search is therefore restricted to the points $P \in S_A$ defined by $P = l \cap l'$, where l' is the set of points having zero radial velocity with respect to the Earth

$$l' = \{(r_2, \dot{r}_2) \in S_A,\, (r_2, \dot{r_2}) \in \dot{\Gamma}_2^s | \dot{r}_2 = 0\}. \tag{10}$$

As at this stage a first guess solution is designed to be later optimized, orbits sufficiently close to P can also be considered. In particular, points $P' \in S_A$ are considered as well, such that $|P' - P| \leq \varepsilon$, where ε is a certain prescribed distance. (Numerical experiment show that values of ε ranging from 10^{-6} to 10^{-5} guarantee convergence of subsequent optimizations). A number of P' points can be generated by varying φ_A. These points, flown forward, generate orbits that are close to $W^s(\gamma_2)$ until the region about γ_2 is reached. From this point on, the orbits get close to $W^u(\gamma_2)$, and their intersection with S_B is studied. The set labeled $\mathcal{E}_{SE}$, $\mathcal{E}_{SE} \in S_B$, represents the set of orbits close to $W^u(\gamma_2)$ whose pre-image $\mathcal{E}_{SE}^{-1}$, $\mathcal{E}_{SE}^{-1} \in S_A$, is made up by P' points. Trajectories defined on $\mathcal{E}_{SE}^{-1}$, $\mathcal{E}_{SE}$, are of interest, as they lead to ballistic escape orbits.

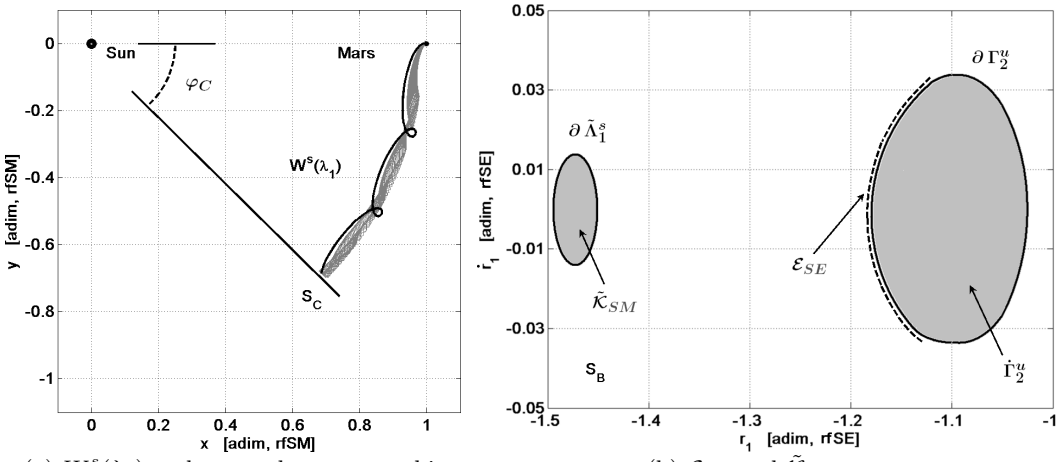

(a) $W^s(\lambda_1)$ and a sample capture orbit. (b) $\mathcal{E}_{SE}$ and $\tilde{\mathcal{K}}_{SM}$ sets.

Fig. 5 Stable manifold $W^s(\lambda_1)$, its section curve $\partial\tilde{\Lambda}_1^s$, Mars-capture set $\tilde{\mathcal{K}}_{SM}$, and the Earth-escape set $\mathcal{E}_{SE}$. Note that if $\mathcal{E}_{SE}$ and $\tilde{\mathcal{K}}_{SE}$ intersected (i.e., $\mathcal{E}_{SE} \cap \tilde{\mathcal{K}}_{SM} \neq \emptyset$), low energy Earth–Mars transfers with at most one deep-space maneuver would exist.

2.4.1 Ballistic Escape with Lunar Gravity Assist

The set $\mathcal{E}_{SE}$ is obtained in the SE RTBP. When the set $\mathcal{E}_{SE}$ is integrated in the Moon-perturbed SE model, its pre-image $\mathcal{E}_{SE}^{-1}$ shows negligible differences with that obtained in the RTBP. However, there are some orbits in $\mathcal{E}_{SE}$ that experience close encounters with the Moon. With the values of φ_A given above, close encounters with the Moon take place at $\theta \in [-\pi/3, -\pi/6]$, where θ is the phase angle of the Moon in Eq. (8). For these orbits, the points $P' \in S_A$ have almost the same coordinates $(r_2, \dot{r}_2)$ as before, but the tangential velocity reduces significantly. More specifically, when a lunar gravity assist is explicitly taken into account, the difference in energy level between the parking orbit and the orbit on $\mathcal{E}_{SE}^{-1}$ is reduced. This yields a lower Δv_E needed to place the orbit on a trans-Martian transfer. On the other hand, the effect of the Moon-perturbation is negligible when the spacecraft flies far from the Earth (the two-body model is already a suitable approximation of the problem, as discussed in [11]). In Fig. 5(b) the set $\mathcal{E}_{SE}$ is reported. In the RTBP, this set is supposed to be inside $\partial\Gamma_2^u$. When the orbits are integrated in the Moon-perturbed SE model, the lunar gravity assist let $\mathcal{E}_{SE}$ to go *outside* $\partial\Gamma_2^u$.

2.5 Ballistic Capture at Mars

Ballistic capture at Mars is designed in analogy with ballistic escape from the Earth. To approach Mars from the interior, a capture via L_1 is considered. In the SM model, the energy level is restricted to values $C_{SM} \lesssim C_1$ such that λ_1 exists, and the Hill's regions are opened at L_1. The manifold $W^s(\lambda_1)$ is computed until a certain surface of section is reached. Section S_C, making an angle φ_C (clockwise) with the x-axis and passing through the Sun, is considered to cut $W^s(\lambda_1)$ (in Fig. 5(a), $\varphi_C = \pi/4$). The corresponding section curve, $\partial\Lambda_1^s$, is represented in $(r_1, \dot{r}_1)$ coordinates. The set $\mathcal{K}_{SM} = \dot{\Lambda}_2^s$ is defined, where $\dot{\Lambda}_1^s \in S_C$ is the set of points inside $\partial\Lambda_1^s$. The points belonging to $\mathcal{K}_{SM}$ are the ones that lead to Mars ballistic capture. These indeed generate orbits inside $W^s(\lambda_1)$ that are the only ones that approach Mars from the interior.

The set $\mathcal{K}_{SM}$ is defined on section S_C in the SM model. However, it is possible to represent $\mathcal{K}_{SM}$ on S_B defined in the SE model through a transformation $\tilde{\mathcal{K}}_{SM} = \mathcal{M}(\mathcal{K}_{SM})$. The operator $\mathcal{M}$ maps states on S_C (SM model) to states on S_B (SE model). It is constructed in five steps: *i*)

the states of the SM model are written in the inertial reference frame with origin at the Sun–Mars barycenter; *ii*) the scaled variables are transformed into physical coordinates; *iii*) the origin is moved to the Earth; *iv*) the variables are scaled considering the SE physical constants; *v*) the variables are reported into the Sun–Earth rotating frame. The same conversion is also applied to $\partial\Lambda_1^s$, in order to obtain $\partial\tilde{\Lambda}_1^s = \mathcal{M}(\partial\Lambda_1^s)$ on section S_B from section S_C. In Fig. 5(b) both $\tilde{\mathcal{K}}_{SM}$ and $\partial\tilde{\Lambda}_1^s$ are reported.

Considering section S_B alone, Earth–Mars low energy transfers could be defined by $\mathcal{E}_{SE} \cap \tilde{\mathcal{K}}_{SM}$. If this intersection had not been empty, the manifolds of the two systems would have been joined by a single deep-space maneuver performed at the patching point. Unfortunately Fig. 5(b) demonstrates that this intersection does not happen, nor it occurs in short-scale times [15]. (In [43] it is shown that these orbits may match in million years, which is not likely the case of real space missions). In [11], a two-impulse strategy was proposed to match the two manifolds. In [24], a low-thrust halo-to-halo rendez-vous was obtained. In [44], Earth–Mars halo-to-halo transfers are designed by applying impulsive maneuvers at the periapsis of the manifolds. In this work, low-thrust capture down to low-altitude orbits about Mars is proposed. This is achieved through the introduction of low-thrust propulsion and the definition of special attainable sets.

3 Low-Thrust Propulsion and Attainable Sets

3.1 The Controlled, Planar Circular Restricted Three-Body Problem

To model the motion of a massless particle P_3 under both the gravitational attractions of P_1, P_2, and the low-thrust propulsion, the controlled RTBP is introduced

$$\ddot{x} - 2\dot{y} = \frac{\partial\Omega}{\partial x} + \frac{T_x}{m}, \quad \ddot{y} + 2\dot{x} = \frac{\partial\Omega}{\partial y} + \frac{T_y}{m}, \quad \dot{m} = -\frac{T}{I_{sp}\, g_0}, \tag{11}$$

where $T = (T_x^2 + T_y^2)^{1/2}$ is the thrust magnitude, I_{sp} the specific impulse of the thruster, and g_0 the Earth gravitational acceleration at sea level. Continuous variations of the spacecraft mass, m, are taken into account through the last of Eqs. (11). This increases the system order by one, and causes a singularity when $m \to 0$ (in addition to the well-known singularities arising when P_3 collides with P_1 or P_2).

The thrust law $\mathbf{T}(t) = (T_x(t), T_y(t))^{\mathrm{T}}$, $t \in [t_i, t_f]$, in Eqs. (11) is not given like in [22, 23], but rather in this approach it represents an unknown that is found by solving an optimal control problem (t_i, t_f are the initial, final times, respectively). $\mathbf{T}$ is determined in such a way that a certain state is targeted and a certain objective function is minimized at the same time. However, at this stage the profile of $\mathbf{T}$ over time is assigned to build first guess solutions. Attainable sets can be defined under this assumption.

3.2 Definition of Attainable Sets

Let $\mathbf{y}_i$ be a vector representing a generic initial state, $\mathbf{y}_i = (x_i, y_i, \dot{x}_i, \dot{y}_i, m_i)$, and let $\phi_{\mathbf{T}(\tau)}(\mathbf{y}_i, t_i; t)$ be the flow of system of Eqs. (11) at time t starting from $(\mathbf{y}_i, t_i)$ and considering the thrust profile $\mathbf{T}(\tau)$, $\tau \in [t_i, t]$. With this notation, it is possible to define the generic point of a low-thrust trajectory through

$$\mathbf{y}(t) = \phi_{\overline{\mathbf{T}}}(\mathbf{y}_i, t_i; t), \tag{12}$$

where $\overline{\mathbf{T}}(t)$ is the thrust law assigned. The low-thrust orbit, at time t, can be expressed as

$$\gamma_{\overline{\mathbf{T}}}(\mathbf{y}_i, t) = \{\phi_{\overline{\mathbf{T}}}(\mathbf{y}_i, t_i; \tau) | \tau < t\}, \tag{13}$$

where the dependence on the initial state $\mathbf{y}_i$ is kept. The attainable set, at time t, can be defined as

$$\mathcal{A}_{\overline{\mathbf{T}}}(t) = \bigcup_{\mathbf{y}_i \in \mathcal{Y}} \gamma_{\overline{\mathbf{T}}}(\mathbf{y}_i, t), \tag{14}$$

where $\mathcal{Y}$ is a domain of admissible initial conditions. Attainable set in Eq. (14) is associated with a generic $\mathcal{Y}$; this set can be defined for the low-thrust capture at Mars (see Section 4).

The thrust law in Eq. (12) is now tailored for the problem at hand. When the spacecraft flies in heliocentric orbit, the low-thrust propulsion is used to *rendez-vous* with Mars. In this context the thrust is aligned with the velocity vector expressed in Sun-centered inertial coordinates. This strategy increases the semimajor axis in a given time. When the spacecraft approaches Mars, the low-thrust is used to achieve *planet capture*, and therefore the velocity is aligned with the velocity expressed in the Sun–Mars rotating frame. This tangential thrust is opposite to the velocity to maximize the variation of Jacobi energy. This is desirable to close the Hill's curves and stabilize the spacecraft about Mars. The thrust law used to define attainable sets is therefore

$$\begin{cases} \overline{\mathbf{T}}(t) = \overline{T}\,(\mathbf{v} + \mathbf{r}^{\perp})/|\mathbf{v} + \mathbf{r}^{\perp}|, & t \in [t_i, t_{\mathrm{rv}}] \\ \overline{\mathbf{T}}(t) = -\overline{T}\,\mathbf{v}/|\mathbf{v}|, & t \in [t_{\mathrm{rv}}, t_{\mathrm{pc}}] \end{cases} \tag{15}$$

where $\mathbf{v} = (\dot{x}, \dot{y})$, $\mathbf{r}^{\perp} = (-y, x)$, and $t_{\mathrm{rv}} - t_i$, $t_{\mathrm{pc}} - t_{\mathrm{rv}}$ are the durations of the rendez-vous and planet capture phases, respectively. The term $\mathbf{v} + \mathbf{r}^{\perp}$ is the velocity expressed in the heliocentric inertial frame [22]. It is worth mentioning that the assigned guidance law in Eq. (15) will be let free to vary in the subsequent optimization step.

Thanks to the definition of $\mathcal{A}_{\overline{\mathbf{T}}}(t)$, low-thrust propulsion can be incorporated in a three-body frame using the same methodology developed for the invariant manifolds. More specifically, invariant manifolds are replaced by attainable sets which are manipulated to find a transfer point on a suitable surface of section. The idea is to mimic the role played by invariant manifolds. This is explained below.

4 Constructing Earth–Mars Transfers with Ballistic Escape and Low-Thrust Capture

The Earth–Mars transfer is made up by a ballistic escape orbit followed by a low-thrust rendez-vous and subsequent planet capture at Mars. The ballistic escape orbit is constructed in the SE model through the method explained in Section 2.4. Low-thrust rendez-vous and capture is instead obtained in the SM model with Eqs. (11) and using attainable sets (Section 3). The preliminary solution is defined by patching together these two "building blocks". The only task left is to specialize the domain of admissible conditions $\mathcal{Y}$ in Eq. (14) needed to define attainable sets.

The transfer ends when the spacecraft reaches the periapsis of the final orbit around Mars. Eccentricity and periapsis (apoapsis) radius of this orbit are fixed. The final state (i.e., the periapsis point) is function of the argument of periapsis, $\mathbf{y}_f = \mathbf{y}_f(\omega_M)$. The domain of admissible final states is

$$\mathcal{Y}^M = \{\mathbf{y}_f(\omega_M) \,|\, \omega_M \in [0, 2\pi]\}. \tag{16}$$

The attainable sets for low-thrust capture are integrated backward starting from $\mathbf{y}_f$ with the control law in Eq. (15). Thus, for some $t = (t_{\mathrm{rv}} - t_i) + (t_{\mathrm{pc}} - t_{\mathrm{rv}})$, the attainable set containing low-thrust rendez-vous and capture trajectories is

$$\mathcal{A}^M_{\overline{\mathbf{T}}}(-t) = \bigcup_{\mathbf{y}_f \in \mathcal{Y}^M} \gamma_{\overline{\mathbf{T}}}(\mathbf{y}_f(\omega_M), -t). \tag{17}$$

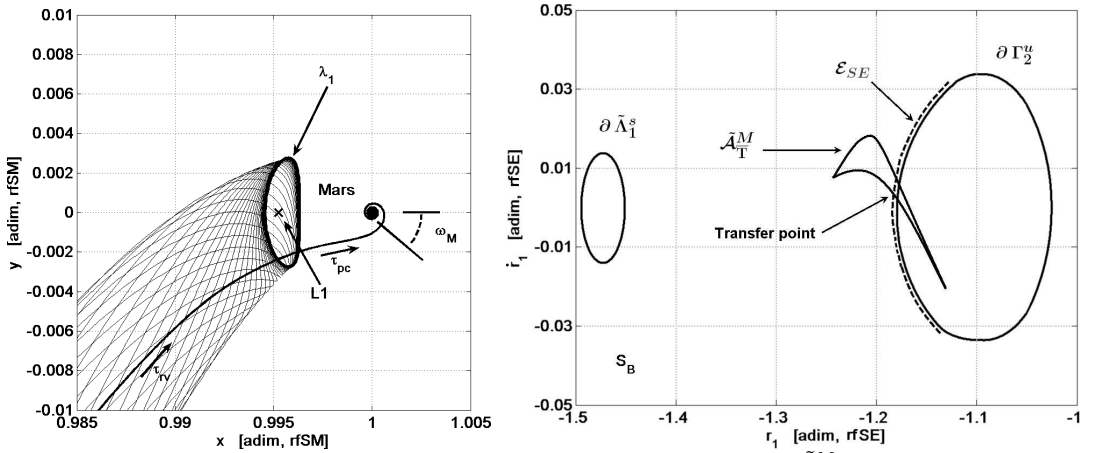

(a) Sample low-thrust capture trajectory. (b) $\mathcal{E}_{SE}$ and $\tilde{\mathcal{A}}^M_{\mathbf{T}}(-t)$ sets.

Fig. 6 A first guess low-thrust capture at Mars and the transfer point $\mathcal{T}^M_{-t} = \mathcal{E}_{SE} \cap \tilde{\mathcal{A}}^M_{\mathbf{T}}(-t)$. By comparing Fig. 5(b) with Fig. 6(b), it is evident that introducing low-thrust capture allows having an intersection (and therefore a transfer point) which was missing with ballistic capture.

Since the first part of the transfer is defined on $\mathcal{E}_{SE}$ (Section 2.4), the transfer points, if any, that generate low-energy, low-thrust Earth–Mars transfers are defined by

$$\mathcal{T}^M_{-t} = \mathcal{E}_{SE} \cap \tilde{\mathcal{A}}^M_{\mathbf{T}}(-t), \tag{18}$$

where $\tilde{\mathcal{A}}^M_{\mathbf{T}}(-t)$ stands for $\mathcal{A}^M_{\mathbf{T}}(-t)$ mapped into the SE model through the map $\mathcal{M}$ in Eq. (**??**). A sample low-thrust capture trajectory and the associated attainable set are reported in Fig. 6. As first guess solutions are being generated with Eq. (18) (to be later optimized in the n-body model), small discontinuities can be again tolerated when looking for the transfer point. This means that it is possible to consider two states such that $\|\mathbf{y}_A - \mathbf{y}_E\| \leq \varepsilon$, where $\mathbf{y}_E \in \mathcal{E}_{SE}$, $\mathbf{y}_A \in \tilde{\mathcal{A}}^M_{\mathbf{T}}(t)$, and ε is a prescribed tolerance. The greater ε is, the higher number of first guess solutions is found; however, ε should be kept sufficiently small to permit the convergence of the subsequent optimization step. Again, values of ε of about 10^{-6} have been considered in this work.

5 Trajectory Optimization in the n-Body Problem

5.1 The Controlled, Restricted n-Body Problem

Once feasible first guess solutions are found, they are optimized in a n-body problem frame. Assuming that the trajectories of the planets are given, the controlled, restricted n-body problem describing the spacecraft motion is

$$\begin{aligned}
\ddot{X} &= \sum_{j \in \mathcal{B}} G\, \frac{m_j}{R_j^3}(X_j - X) + \frac{T_X}{m}, \\
\ddot{Y} &= \sum_{j \in \mathcal{B}} G\, \frac{m_j}{R_j^3}(Y_j - Y) + \frac{T_Y}{m}, \\
\ddot{Z} &= \sum_{j \in \mathcal{B}} G\, \frac{m_j}{R_j^3}(Z_j - Z) + \frac{T_Z}{m}, \\
\dot{m} &= -\frac{T}{I_{sp}\, g_0},
\end{aligned} \tag{19}$$

where $\mathbf{R} = (X, Y, Z)$ and $\mathbf{R}_j = (X_j, Y_j, Z_j)$ are the positions of both the spacecraft and the j-th planet, respectively, expressed in an inertial reference frame; $R_j = |\mathbf{R}_j - \mathbf{R}|$, G is the universal gravitational constant, and m_j is the mass of the j-th planet. In Eqs. (19), $\mathcal{B}$ is the set containing the celestial bodies of interest; i.e., $\mathcal{B} = \{\text{Sun}, \text{Earth}, \text{Moon}, \text{Mars}\}$. The last of Eqs. (19) is needed to introduce the low-thrust control, and to take into account the variation of the spacecraft mass m. The analytical ephemeris model provides the positions of the primaries as functions of time, i.e., $X_j = X_j(t)$, $Y_j = Y_j(t)$, $Z_j = Z_j(t)$. This model is an approximation of JPL ephemeris DE405, where the positions of the planets are given as third-order polynomial of the epoch. It has been shown that such model is quite accurate for preliminary trajectory design purposes [45].

The low-thrust version of the classic restricted n-body problem consists of a seventh-order system of differential equations which describe the *spatial* problem. The spacecraft is allowed to move in three dimensions and the real eccentricities and orbital inclinations of the planets are considered. This model is therefore more accurate than the three-/four-body problems used to derive the first guess solutions. Thus, in the optimization step, first guesses are both improved (from a performance index point of view) and refined (from a dynamical model point of view).

5.2 Optimal Control Problem Statement

The optimal control problem is divided into three different stages according to the formalism proposed in [46, 47]. This is because solving the ballistic escape, the heliocentric phase, and the low-thrust capture, all with Eqs. (19) is not efficient as the terms R_j show variations of several orders of magnitude. The n-body problem equations of motion are therefore written in frames centered at the Earth, Sun, and Mars. The three stages in which the optimal control problem is subdivided are: departure from the Earth; heliocentric orbit; arrival at Mars. Let $\mathbf{y} = (x, y, z, \dot{x}, \dot{y}, \dot{z}, m)$ be a generic state. Without loosing any generality, the stage notation is not used for the sake of brevity.

The optimal control problem aims at finding the guidance law, $\mathbf{T}(t)$, $t \in [t_i, t_f]$, that minimizes the following performance index

$$J = \rho\, \Delta v_E + \int_{t_i}^{t_f} \frac{T(t)}{I_{sp}\, g_0}\, \mathrm{d}t, \tag{20}$$

where Δv_E is the magnitude of the Earth-escape maneuver. The second contribution to the objective function is the propellant mass, m_p, spent in the low-thrust phase. (This can be derived by integrating the last of Eqs. (19)). The parameter ρ is a weight quantity introduced to balance the two contributions in the objective function.

The left boundary condition has to constrain the initial state on a circular parking orbit of radius $r_i = R_E + h_E$ about the Earth with velocity perpendicular to the position vector (R_E is the Earth's mean radius). In inertial Earth-centered coordinates, the initial boundary condition reads

$$\boldsymbol{\psi}_i(\mathbf{y}_i, t_i) := \begin{cases} x_i^2 + y_i^2 + z_i^2 = r_i^2, \\ x_i\dot{x}_i + y_i\dot{y}_i + z_i\dot{z}_i = 0. \end{cases} \tag{21}$$

Under these conditions, the magnitude of the trans-Mars injection maneuver is

$$\Delta v_E = \sqrt{\dot{x}_i^2 + \dot{y}_i^2 + \dot{z}_i^2} - \sqrt{\frac{\mu_E}{r_i}} \tag{22}$$

where μ_E is the Earth's gravitational parameter ($\mu_E = 3.986 \times 10^5\,\mathrm{km}^3/\mathrm{s}^2$). Analogously, the final state $\mathbf{y}_f$ expressed in inertial Mars-centered coordinates has to verify the right boundary

condition

$$\boldsymbol{\psi}_f(\mathbf{y}_f, t_f) := \begin{cases} x_f^2 + y_f^2 + z_f^2 = r_f^2, \\ x_f\dot{x}_f + y_f\dot{y}_f + z_f\dot{z}_f = 0 \\ \dot{x}_f^2 + \dot{y}_f^2 + \dot{z}_f^2 = \dfrac{\mu_M(1+e)}{r_f} \end{cases} \tag{23}$$

where r_f and e are the periapsis radius and the eccentricity of the final orbit about Mars, respectively; μ_M is the gravitational parameter of Mars ($\mu_M = 4.282 \times 10^4\,\mathrm{km}^3/\mathrm{s}^2$). In addition, the following path constraint is imposed

$$T(t) \leq T_{max}, \tag{24}$$

to model the saturation of the low-thrust engine. Eqs. (20)–(24) define the optimal control problem for the Earth–Mars transfer. This problem may be solved with a variety of methods. In this work we have faced it with direct transcription and multiple shooting.

5.3 Solution by Direct Transcription and Multiple Shooting

The optimal control problem is transcribed into a nonlinear programming problem by means of a direct approach [48]. This method generally shows robustness and versatility, and does not require explicit derivation of the necessary conditions of optimality; its convergence to a final solutions is also less sensitive to variations of the first guess solutions [46]. More specifically, a multiple shooting scheme is implemented [49]. With this strategy, the n-body equations of motion are forward integrated within $N-1$ intervals in which $[t_i,\, t_f]$ is split. This is done assuming N points and constructing the mesh $t_i = t_1 < \cdots < t_N = t_f$. The solution is discretized over these N grid nodes; i.e, $\mathbf{y}_j = \mathbf{y}(t_j)$. The matching of position, velocity, and mass is imposed at the endpoints of the intervals in the form of defects as

$$\boldsymbol{\eta}_j = \bar{\mathbf{y}}_j - \mathbf{y}_{j+1} = 0, \qquad j = 1, \ldots, N-1 \tag{25}$$

with $\bar{\mathbf{y}}_j = \phi_{\mathbf{T}(\tau)}(\mathbf{y}_j, t_j; t_{j+1})$, $\tau \in [t_j,\, t_{j+1}]$. This is done in each of the three stages in which the problem is divided, and matching of position, velocity, and mass is also imposed at their endpoints. To compute $\mathbf{T}(\tau)$ a second-level time discretization is implemented by splitting each of the $N-1$ intervals into $M-1$ subsegments. The control is discretized over the M subnodes; i.e., $\mathbf{T}_{j,k}$, $j = 1, \ldots, N$, $k = 1, \ldots, M$. A third-order spline interpolation is achieved by selecting $M = 4$. Initial and final time t_1, t_N, are included into the nonlinear programming variable, so allowing the optimization of variable-time transfers.

The transcribed nonlinear programming problem finds the states and the controls at mesh points ($\mathbf{y}_j$ and $\mathbf{T}_{j,k}$) in the respect of Eqs. (21)–(24) and minimizing the performance index (Eq. (20)). It is worth stressing that not only the initial low-thrust portion, but rather the whole transfer trajectory is discretized and optimized, so allowing the low-thrust to act also in regions preliminarily made up by coast arcs. To find accurate optimal solutions without excessively increasing the computational burden, an adaptive nonuniform time grid has been implemented. When the trajectory is close to either the Earth or Mars the grid is refined, whereas in the intermediate phase, where the Sun attraction mostly governs the motion of the spacecraft, a coarse grid is used. This is done by hand; the implementation of an automatic mesh refinement scheme would be beyond the scopes of the paper. The optimal solution found is assessed a posteriori by forward integrating the optimal initial condition using an eighth-order Runge–Kutta–Fehlberg scheme (tolerance set to 10^{-12}) by cubic interpolation of the discrete optimal control solution.

6 Optimized Transfer Solutions

The optimal transfers presented connect the following orbits

- a circular orbit around the Earth at an altitude of $h_E = 167\,\text{km}$;
- a circular orbit around Mars at an altitude of $h_M = 10000\,\text{km}$.

The latter has been chosen for the sake of comparison (it corresponds to the arrival orbit of a known example where ballistic capture at Mars is studied [11]), though the method is formulated to reach any orbit about Mars once eccentricity and periapsis (apoapsis) altitude are specified. The results are summarized in Table 1 where 'fg' is the first guess and 'sol' is the corresponding optimized solution. Last two rows represent the reference, impulsive solutions.

Table 1 is organized as follows. In the second column, Δv_E is the magnitude of the initial impulsive maneuver. This is a direct output of the optimization step and is calculated through Eq. (22). In the third column, Δv_M is the magnitude of all impulsive maneuvers needed to reach the final orbit around Mars (this applies to the second reference solutions only, where three maneuvers are considered). In the fourth column, f_f is the propellant mass fraction needed for the rendez-vous and the low-thrust capture (this number does not take into account the initial impulsive maneuver). For the optimized transfers, f_f is calculated as

$$f_F = \frac{1}{m_{TM}} \int_{t_i}^{t_f} \frac{T(t)}{I_{sp}\, g_0}\, \mathrm{d}t, \tag{26}$$

where m_{TM} is the mass injected into the trans-Mars orbit ($m_{TM} = 1000\,\text{kg}$). For the reference solution, f_f is calculated as

$$f_f = 1 - \exp\left(-\frac{\Delta v_M}{I_{sp}^{ht}\, g_0}\right), \tag{27}$$

where $I_{sp}^{ht} = 300\,\text{s}$ is the specific impulse of high-thrust engines. In the fifth column, f_t represents the overall mass fraction necessary to carry out the transfer. For the optimized solutions, f_t is calculated through

$$f_t = \frac{m_p}{m_i} = \left[1 - \exp\left(-\frac{\Delta v_E}{I_{sp}^{ht}\, g_0}\right)\right] + \frac{1}{m_i} \int_{t_i}^{t_f} \frac{T(t)}{I_{sp}^{lt}\, g_0}\, \mathrm{d}t, \tag{28}$$

where m_i is the initial mass (calculated to inject $m_{TM} = 1000\,\text{kg}$ with a Δv_E maneuver), and $I_{sp}^{lt} = 3000\,\text{s}$ is the specific impulse of the low-thrust engines. The transfer time, Δt, is reported in the sixth column. A maximum available thrust of $T_{max} = 0.25\,\text{N}$ has been considered in Eq. (24). Sol 2 is reported in Fig. 7.

6.1 Discussion

In Table 1, the two optimized solutions show a shorter flight time and a higher mass consumption than the corresponding first guesses. This is because the optimal control problem spreads the discontinuity at the transfer point P; more propellant than the first guess is spent, and the flight time is shorten. In addition, sol 2 outperforms sol 1 in terms of both flight time and Δv_E. This is due to the fact that fg 2 is designed to take explicitly advantage of a lunar flyby (see Fig. 7(c)). This feature reduces the magnitude of Δv_E by 110 m/s and gives reasons for the introduction of the Moon-perturbed SE model presented in Section 2.3. Moreover, the flight time is reduced by shrewdly tuning the angles φ_B, φ_C that define the plane where $\mathcal{T}_{-t}^{M} = \mathcal{E}_{SE} \cap \tilde{\mathcal{A}}_{\mathbf{T}}^{M}(-t)$ is defined.

Optimized solutions offer lower overall mass fraction f_t than reference solutions. This happens for two reasons. Firstly, I_{sp}^{lt} is one order of magnitude greater than I_{sp}^{ht}. Secondly, the first guess

Table 1 Low-energy, low-thrust transfers to low-Mars orbits. First guesses and their optimized solutions are reported together with two impulsive reference solutions (H: Hohmann).

Type	Δv_E [m/s]	Δv_M [m/s]	f_f [adim.]	f_t [adim.]	Δt [days]
fg 1	3260	–	0.150	0.719	756
fg 2	3150	–	0.150	0.709	553
sol 1	3253	–	0.199	0.734	703
sol 2	3141	–	0.200	0.724	496
H	3620	1878	0.472	0.846	259
[11]	3554	1915	0.478	0.844	823

solutions exploit the dynamics of the three-/four-body problems in which they are designed, and the optimized solutions efficiently use the 5-body problem accordingly. The flight times lie between those of the reference transfers. From Fig. 7(e) it can be inferred that the thrust profile respects the saturation constraint described by Eq. (24). The control profile recalls an on-off structure, which is valid for both the rendez-vous and low-thrust capture phases. We expect that with arrival and departure orbits with nonzero eccentricity, the structure of the transfer would not be too different from the solutions presented in this study, though a shorter flight time and a lower propellant mass fraction could be achieved. As for the inclination of the departure and arrival orbits, the optimized solution may have nonzero inclination (± 15 deg determined through numerical experiments) even though the first guess is planar. If polar orbits about Mars are of interest, the described method is still valid provided that the first guess is constructed starting from high inclined arrival orbits.

7 Conclusions

A method to incorporate low-thrust propulsion into standard invariant manifold technique to design interplanetary transfers has been presented in this paper. This is done through the definition of special attainable sets that are manipulated together with invariant manifolds. This procedure recalls the one used in the patched restricted three-body problems approximation, and uses attainable sets to fill the gap in systems with nonintersecting manifolds (Sun–Earth and Sun–Mars systems in this case). The proposed transfers are made up by three phases: a ballistic escape, a low-thrust planetary rendez-vous, and a low-thrust capture. The ballistic escape exploits both a lunar gravity assist and the Sun–Earth gravitational attractions. This is defined in a special Moon-perturbed Sun–Earth problem developed purposely. The method has been specialized to Earth–Mars transfers although it can be used in a broader context. Efficient solutions have been shown to support the validity of the presented approach.

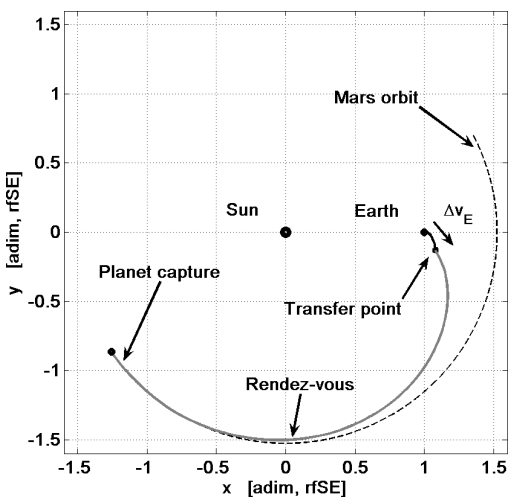

(a) First guess solution (SE reference frame).

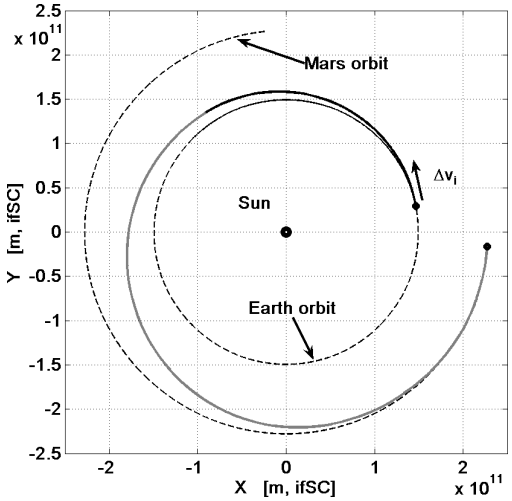

(b) Optimal trajectory (heliocentric frame).

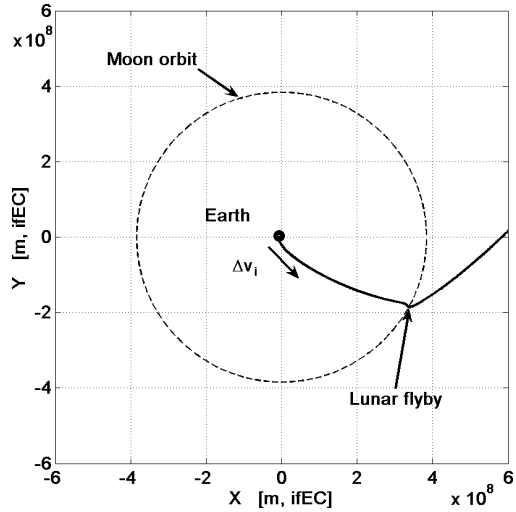

(c) Ballistic escape with lunar gravity assist (inertial Earth-centered frame).

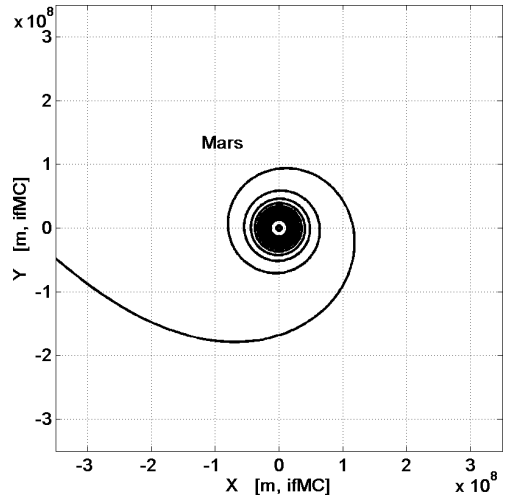

(d) Low-thrust capture (inertial Mars-centered frame).

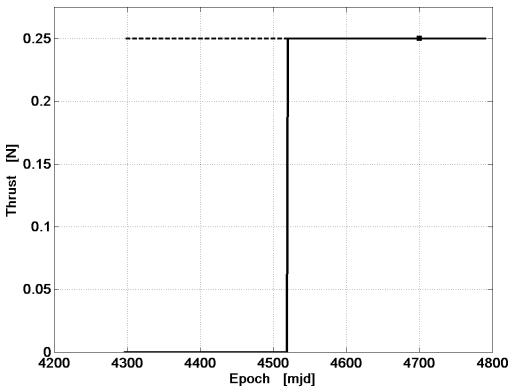

(e) Optimal guidance law.

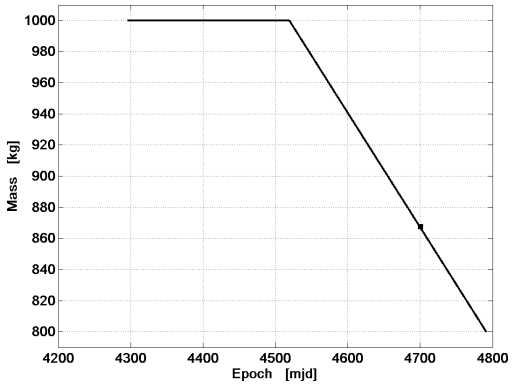

(f) Mass consumption trend.

Fig. 7 The optimized transfer corresponding to sol 2 in Table 1.

References

1. E. Belbruno. *Capture Dynamics and Chaotic Motions in Celestial Mechanics: With Applications to the Construction of Low Energy Transfers*. Princeton University Press, Princeton, NJ, 2004.
2. E. Belbruno and J. Miller. Sun-Perturbed Earth-to-Moon Transfers with Ballistic Capture. *Journal of Guidance, Control, and Dynamics*, 16:770–775, 1993.
3. E. Belbruno. The Dynamical Mechanism of Ballistic Lunar Capture Transfers in the Four-Body Problem from the Perspective of Invariant Manifolds and Hill's Regions. In *Technical Report, Centre De Recerca Matematica, Barcelona, Spain*, 1994.
4. M.W. Lo and S.D. Ross. Low Energy Interplanetary Transfers using the Invarian Manifolds of L_1, L_2, and Halo Orbits . In *Paper AAS 98-136, Proceedings of the AAS/AIAA Space Flight Mechanics Meeting*, 1998.
5. W.S. Koon, M.W. Lo, J.E. Marsden, and S.D. Ross. Heteroclinic Connections between Periodic Orbits and Resonance Transitions in Celestial Mechanics. *Chaos*, 10:427–469, 2000.
6. G. Gómez, W.S. Koon, M.W. Lo, J.E. Marsden, J. Masdemont, and S.D. Ross. Invariant Manifolds, the Spatial Three-Body Problem and Space Mission Design. *Advances in the Astronautical Sciences*, 109:3–22, 2001.
7. W.S. Koon, M.W. Lo, J.E. Marsden, and S.D. Ross. Low Energy Transfer to the Moon. *Celestial Mechanics and Dynamical Astronomy*, 81:63–73, 2001.
8. G. Gómez, J. Masdemont, and J.M. Mondelo. Libration Point Orbits: A Survey from the Dynamical Point of View. In *Proceedings of the International Conference on Libration Point Orbits and Applications*, Girona, Spain, 2002.
9. W.S. Koon, M.W. Lo, J.E. Marsden, and S.D. Ross. Constructing a Low Energy Transfer between Jovian Moons. *Contemporary Mathematics*, 292:129–145, 2002.
10. J.E. Marsden and S.D. Ross. New Methods in Celestial Mechanics and Mission Design. *Bulletin of the American Mathematical Society*, 43:43–73, 2006.
11. F. Topputo, M. Vasile, and F. Bernelli-Zazzera. Low Energy Interplanetary Transfers Exploiting Invariant Manifolds of the Restricted Three-Body Problem. *Journal of the Astronautical Sciences*, 53:353–372, 2005.
12. E. Belbruno. Examples of the Nonlinear Dynamics of Ballistic Capture and Escape in the Earth–Moon System. In *AIAA paper 90-2896, AIAA Astrodynamics Conference, Portland, Oregon*, 1990.
13. F. Topputo, E. Belbruno, and M. Gidea. Resonant Motion, Ballistic Escape, and their Applications in Astrodynamics. *Advances in Space Research*, 42(8):6–17, October 2008.
14. F. Topputo, M. Vasile, and F. Bernelli-Zazzera. A Hybrid Optimization of the Low Energy Interplanetary Transfers Associated to the Invariant Manifolds of the Restricted Three-Body Problem. In *Paper IAC-04-A.6.06, 55th International Astronautical Congress, Vancouver, Canada, 4-8 October*, 2004.
15. Y. Ren, J. Masdemont, G. Gómez, and E. Fantino. Two Mechanism of Natural Transport in the Solar System. *Computations in Nonlinear Science and Numerical Simulations*, to appear, 2011.
16. F. Topputo. *Low-Thrust Non-Keplerian Orbits: Analysis, Design, and Control*. PhD thesis, Politecnico di Milano, Milano, Italy, 2007.
17. G. Mingotti. *Trajectory Design and Optimization in Highly Nonlinear Astrodynamics*. PhD thesis, Politecnico di Milano, Milano, Italy, 2010.
18. E. Belbruno. Lunar Capture Orbits, a Method of Constructing Earth–Moon Trajectories and the Lunar GAS Mission. In *Paper AIAA 97-1054, Proceedings of the 19th AIAA/DGLR/JSASS International Electric Propulsion Conference, Colorado Springs, CO*, 1987.
19. J. Schoenmaekers, D. Horas, and J.A. Pulido. SMART-1: With Solar Electric Propulsion to the Moon. In *Proceedings of the 16th International Symposium on Space Flight Dynamics, Pasadena, CA*, 2001.
20. R.L. Anderson and M.W. Lo. Role of Invariant Manifolds in Low-Thrust Trajectory Design. *Journal of Guidance, Control, and Dynamics*, 32:1921–1930, 2009.
21. G.J. Whiffen and J.A. Sims. Application of the SDC Optimal Control Algorithm to Low-Thrust Escape and Capture Trajectory Optimization. *Advances in the Astronautical Sciences*, 112:1361–1382, 2002.
22. M. Dellnitz, O. Junge, M. Post, and B. Thiere. On Target for Venus – Set Oriented Computation of Energy Efficient Low Thrust Trajectories. *Celestial Mechanics and Dynamical Astronomy*, 95: 357–370, 2006.
23. M. Dellnitz, K. Padberg, M. Post, and B. Thiere. Set Oriented Approximation of Invariant Manifolds: Review of Concepts for Astrodynamical Problems. *American Institute of Physics Conference Proceedings*, 886:90–99, 2007.
24. P. Pergola, K. Geurts, C. Casaregola, and M. Andrenucci. Earth–Mars Halo to Halo Low Thrust Manifold Transfers. *Celestial Mechanics and Dynamical Astronomy*, 105:19–32, 2009.
25. G. Mingotti, F. Topputo, and F. Bernelli-Zazzera. Low-Energy, Low-Thrust Transfers to the Moon. *Celestial Mechanics and Dynamical Astronomy*, 105:61–74, 2009.

26. G. Mingotti, F. Topputo, and F. Bernelli-Zazzera. Numerical Methods to Design Low-Energy, Low-Thrust Sun-Perturbed Transfers to the Moon. In *Proceedings of the 49th Israel Annual Conference on Aerospace Sciences, Tel Aviv – Haifa, Israel*, 2009.
27. T.F. Starchville and R.G. Melton. Optimal Low-Thrust Trajectories to Earth-Moon L_2 Halo Orbits (Circular Problem). In *Paper AAS 97-714, Proceedings of the AAS/AIAA Astrodynamics Specialists Conference, Sun Valley, ID*, 1997.
28. T.F. Starchville and R.G. Melton. Optimal Low-Thrust Transfers to Halo Orbits about the L2 Libration Point in the Earth-Moon System (Elliptical Problem). *Advances in the Astronautical Sciences*, 99(2):1489–1505, 1998.
29. A. Sukhanov and N. Eismont. Low Thrust Transfer to Sun-Earth L_1 and L_2 Points with a Constraint on the Thrust Direction. In *Proceedings of the International Conference on Libration Point Orbits and Applications, Girona, Spain,*, 2002.
30. J. Senent, C. Ocampo, and A. Capella. Low-Thrust Variable-Specific-Impulse Transfers and Guidance to Unstable Periodic Orbits. *Journal of Guidance, Control, and Dynamics*, 28:280–290, 2005.
31. G. Mingotti, F. Topputo, and F. Bernelli-Zazzera. Combined Optimal Low-Thrust and Stable-Manifold Trajectories to the Earth–Moon Halo Orbits. *American Institute of Physics Conference Proceedings*, 886:100–110, 2007.
32. K. Howell and M. Ozimek. Low-Thrust Transfers in the Earth-Moon System Including Applications to Libration Point Orbits. In *Paper AAS 07-343, Proceedings of the AAS/AIAA Astrodynamics Specialist Conference, Mackinac Island, MI*, 2007.
33. C. Martin, B.A. Conway, and P. Ibáñez. *Space Manifold Dynamics*, chapter Optimal Low-Thrust Trajectories to the Interior Earth-Moon Lagrange Point, pages 161–184. Springer, 2010.
34. J. Gil-Fernández, C. Corral Van Damme, M. Graziano, G.B. Amata, F. Cogo, and M.A. Perino. ExoMars Alternative Escape Trajectories with Soyuz/Fregat. *Annals of the New York Academy of Sciences*, 1065(1):15–36, 2005.
35. S. Kemble. *Interplanetary Mission Analysis and Design*. Springer, New York, 2006.
36. V. Szebehely. *Theory of Orbits: The Restricted Problem of Three Bodies*. Academic Press Inc., New York, 1967.
37. C.C. Conley. Low Energy Transit Orbits in the Restricted Three-Body Problem. *SIAM Journal on Applied Mathematics*, 16:732–746, 1968.
38. J. Llibre, R. Martínez, and C. Simó. Transversality of the Invariant Manifolds Associated to the Lyapunov Family of Periodic Orbits Near L_2 in the Restricted Three-Body Problem. *Journal of Differential Equations*, 58:104–156, 1985.
39. C. Simó, G. Gómez, A. Jorba, and J. Masdemont. The Bicircular Model near the Triangular Libration Points of the RTBP. In *From Newton to Chaos*, pages 343–370, 1995.
40. D.R. Williams. Planetary Fact Sheets, NASA: National Aeronautics and Space Administration, 2007. http://nssdc.gsfc.nasa.gov/planetary/planetfact.html.
41. G. Gómez, A. Jorba, J. Masdemont, and C. Simó. Study of the Transfer from the Earth to a Halo Orbit around the Equilibrium Point L1. *Celestial Mechanics and Dynamical Astronomy*, 56:239–259, 1993.
42. T.S. Parker and L.O. Chua. *Practical Numerical Algorithms for Chaotic Systems*. Springer, New York, 1989.
43. B.J. Gladman. *Delivery of Planetary Ejecta to Earth*. PhD thesis, Cornell University, Ithaca, NY, 1996.
44. M. Nakamiya, H. Yamakawa, D. Scheeres, and D. Yoshikawa. Interplanetary Transfers between Halo Orbits: Connectivity between Escape and Capture Trajectories. *Journal of Guidance, Control, and Dynamics*, 33:803–813, 2010.
45. R. Armellin, P. Di Lizia, F. Topputo, M. Lavagna, F. Bernelli-Zazzera, and M. Berz. Gravity Assist Space Pruning based on Differential Algebra. *Celestial Mechanics and Dynamical Astronomy*, 106 (1):1–24, 2010.
46. J.T. Betts. Survey of Numerical Methods for Trajectory Optimization. *Journal of Guidance, Control, and Dynamics*, 21:193–207, 1998.
47. J.T. Betts. *Practical Methods for Optimal Control Using Nonlinear Programming*. SIAM, 2000.
48. C. Hargraves and S. Paris. Direct Trajectory Optimization Using Nonlinear Programming and Collocations. *Journal of Guidance, Control, and Dynamics*, 10:338–342, 1987.
49. P.J. Enright and B.A. Conway. Discrete Approximations to Optimal Trajectories Using Direct Transcription and Nonlinear Programming. *Journal of Guidance, Control, and Dynamics*, 15:994–1002, 1992.